

A Redox-active Manganate(0) Dicarbene Metalloradical

Ageliki Karagiannis,^a Alexei M. Tyryshkin,^b Roger A. Lalancette,^a Denis M. Spasyuk,^c Asmaa Washington^a and Demyan E. Prokopchuk^{a*}

^aDepartment of Chemistry, Rutgers University – Newark, Newark, NJ 07102, United States. Email: demyan.prokopchuk@rutgers.edu

^bDepartment of Chemistry and Chemical Biology, Rutgers University, Piscataway, NJ 08854, United States

^cCanadian Light Source, Saskatoon, Saskatchewan, S7N2V3, Canada

We report a rare redox-active Mn⁰ metalloradical [Mn(CO)₃(Ph₂B(^tBuNHC)₂)]⁻ (NHC = N-heterocyclic carbene) with counteranions [K([2.2.2]cryptand)]⁺, [Na([2.2.2]cryptand)]⁺, or [Li(DME)(12-crown-4)]⁺, all characterized via single crystal X-ray diffraction. Cyclic voltammograms reveal solvation-dependent Mn^{I/0} redox potentials that are modeled using the Born equation.

There is ongoing interest in developing redox active transition metal complexes for applications in molecular electrocatalysis using Earth-abundant metals such as Ni, Fe, and Co.^[1,2] An equally attractive metal is manganese and several groups have reported Mn^I complexes that are electrocatalytically active for CO₂ reduction to CO^[3,4,5,6] and H⁺ to H₂^[7] via intermediates with a formal Mn^{-I} oxidation state. A key Mn⁰ intermediate is typically proposed, however observing and chemically separating the mononuclear species has proven to be challenging because Mn⁰ complexes readily dimerize to form a Mn—Mn bond, such as in Mn₂(CO)₁₀ and [Mn(CO)₃(tmbp)]₂^[8] (tmbp = 4,4',5,5'-tetramethyl-2,2'-biphosphinine). Likewise, [Mn^I(CO)₃(bis-^{Me}NHC)Br]^[3] and [Mn^I(CO)₃(bpy-^tBu)Br]^[5] (NHC = N-heterocyclic carbene and bpy = bipyridine) suffer from an off-cycle dimerization pathway during the reduction CO₂ to CO in the presence of exogenous acid. In 2014, Kubiak and coworkers used 6,6'-dimesityl-2,2'-bipyridine (mesbpy) to increase the steric bulk of their [Mn(CO)₃(bpyR)Br]^[6] framework, which prevented dimerization.

Despite the importance of Mn⁰ intermediates in small molecule activation and electrocatalysis, only a few structurally characterized monomeric Mn⁰ complexes have been published to date (Fig 1). Figueroa and coworkers reported that the incorporation of two sterically encumbering isocyanide ligands allows the formation of the monoradical [Mn(CO)₃(CNA^{Dipp})₂]^[9] an analogue to the unstable [Mn(CO)₅] monoradical (Dipp = 2,6-diisopropylphenyl), demonstrating atom abstraction and radical scavenger reactivity. Deng and co-workers reported that the inclusion of NHC and alkene ligands gave rise to three-coordinate Mn⁰ complexes [(NHC)Mn(dvtms)]^[10] which are reactive towards H₂ and unsaturated C-C bonds to yield Mn^{II} dialkyl compounds. Furthermore, Tonzetich and coworkers showed that chemical reduction of the Mn^I pyrrole-based pincer complex, [Mn(CO)₂(^tBuPNP)], yields the rare mononuclear low spin Mn⁰ metalloradical, [K][Mn(CO)₂(^tBuPNP)]^[11] Cyclic voltammetry and treatment of [K][Mn(CO)₂(^tBuPNP)] with NO_(g) revealed a facile re-oxidation to the Mn^I precursor, demonstrating the robust nature of this Mn^{I/0} redox couple (E_{1/2} = -2.14 V vs. Fc^{+/0}, THF).

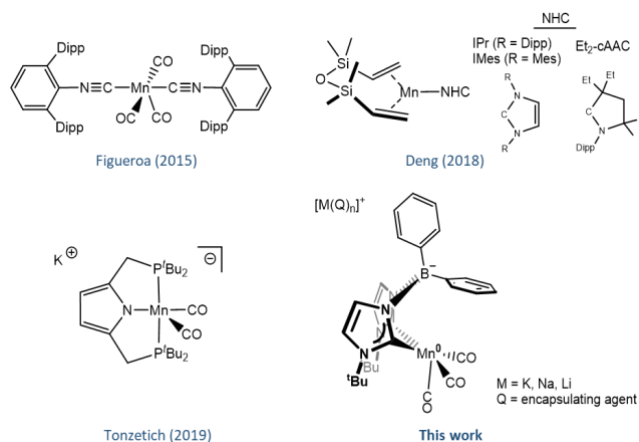
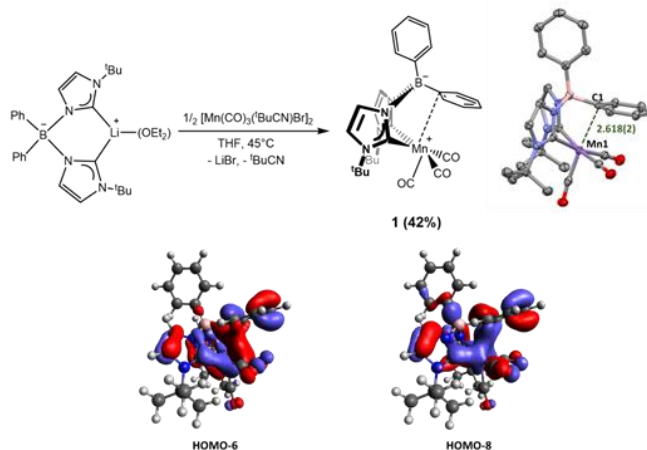


Figure 1. Reported Mn⁰ complexes in the literature and the novel Mn⁰ dicarbene metalloradical. Dipp = 2,6-diisopropylphenyl, Mes = 2,4,6-trimethylphenyl, cAAC = cyclic alkylamino carbene. [M(Q)_n]⁺ denotes counterion M⁺ and encapsulating agent Q.

We describe the synthesis of a rare five-coordinate manganate(0) tricarbonyl complex coordinated to a borate-bridged bis(NHC) ligand that exhibits medium-dependent redox behavior. Starting with a Mn^I precursor, the singly reduced Mn⁰ species can be accessed via cyclic voltammetry or by using alkali metal sources to generate mononuclear manganates. X-ray crystallographic analysis confirms the molecular structure of these distorted trigonal bipyramidal complexes and the spectroscopic properties at Mn remain independent of the encapsulated counterion after crystallization ([K(2,2,2-crypt)]⁺ vs. [Na(2,2,2-crypt)]⁺ vs. [Li(DME)(12-crown-4)]⁺); (DME = 1,2-dimethoxyethane).

The Mn^I complex [Ph₂B(^tBuNHC)₂Mn(CO)₃] (**1**) is synthesized from the lithium carbene [Li(Ph₂B(^tBuNHC)₂•Et₂O)]^[12] and half an equivalent of the bromide-bridged dimer [Mn(CO)₃(^tBuCN)Br]₂^[13] with mild heating (Scheme 1, top). Formation of **1** is sensitive to the Mn source - using MnBr(CO)₅ was unsuccessful, mirroring observations made by Smith and co-workers for chelation of a borate-bridged tris(NHC) ligand to Mn.^[13] Notably, washing the crude product with methanol is essential to remove all traces of LiBr from the product. After workup, red-orange **1** is obtained in 42% yield and was further characterized by single crystal X-ray diffraction (Scheme 1, right). The distance between the Mn atom and arene C_{ipso} atom above the metal center (Mn---C_{ipso} = 2.618(2) Å) is significantly longer than the sum of the Mn—C and Mn—B covalent radii (2.12 and 2.23 Å, respectively)^[14] but shorter than the sum of their van der Waals radii (3.75 and 3.85 Å, respectively).^[15]

Computational analysis (DFT) reveals bonding interactions between the *ipso* and *ortho* carbons of the arene π-system on the ligand, as portrayed in HOMO-6 and HOMO-8 (Scheme 1, bottom). This type of stabilizing interaction is expected because the coordinatively unsaturated Mn center would have only 16 valence e⁻ in the absence of overlap with the π-electron system of the aromatic ring. Solid-state IR spectroscopic data of **1** show CO stretches at 2010, 1928, and 1881 cm⁻¹ which remain identical in solution-phase IR spectroscopy in both MeCN and DCM (Fig S4). Furthermore, UV-vis spectra in CH₂Cl₂ and CH₃CN only show minor differences in molar absorptivity (Fig S12,S13). The observed carbonyl stretches are significantly lower than [Mn(CO)₃(^tBuCN)Br]₂ (2025, 1936, and 1915 cm⁻¹) but similar to those found in the methylene-bridged dicarbene complex [Mn(CO)₃(bis-^MeNHC)Br] (2004, 1912, and 1881 cm⁻¹).^[3]



Scheme 1. Top: Synthesis of **1** and its molecular structure. $\text{Mn}\cdots\text{C}_{\text{ipso}} = 2.618(2) \text{ \AA}$, 50% probability ellipsoids. Hydrogen atoms are omitted for clarity. Bottom: HOMO-6 and HOMO-8 of **1** (TPSS-D3(BJ)/def2-TZVP/CPCM(MeCN); isosurface value = 0.04; see the SI for additional details).

Cyclic voltammograms (CVs) of **1** were conducted under N_2 to examine its solution phase electrochemical activity. CVs in anhydrous MeCN and THF reveal redox events at $E_{1/2} = -1.75 \text{ V}$ and $E_{1/2} = -1.94 \text{ V}$ vs. $\text{Fc}^{+/0}$, respectively (Fig 2). The anodic shift on going from MeCN to a different solvent can be estimated using a modified Born equation^[17,18] where $\Delta\Delta G^\circ$ is expressed in kcal/mol, z is the ionic charge (-1), ϵ is the dielectric constant ($\epsilon_{\text{THF}} = 7.43$, $\epsilon_{\text{MeCN}} = 35.7$),^[19] r_{eff} is the effective spherical ionic radius in \AA , and 166 is a grouping of all other constants (eq 1). The r_{eff} is estimated to be 5.3 \AA based on distances measured from X-Ray structural data for the Mn^0 anion (see below).

$$\Delta\Delta G^\circ(\text{Solv} - \text{MeCN}) = 166 \frac{z^2}{r_{\text{eff}}} \left(\frac{1}{\epsilon_{\text{solv}}} - \frac{1}{\epsilon_{\text{MeCN}}} \right) \quad (1)$$

Using eq. 1, we estimate $\Delta\Delta G^\circ(\text{THF-MeCN}) = -3.3 \text{ kcal/mol}$, or $\Delta E^\circ = 0.15 \text{ V}$, which is in excellent agreement with the observed potential difference of 0.19 V in Figure 2. In addition, CV experiments with varying THF:MeCN ratios show a gradual shift in redox potential between these two extremes (Fig S11). To further validate this interpretation, CVs of **1** in methyl *tert*-butyl ether (MTBE) saturated with $[\text{nBu}_4\text{N}][\text{B}(\text{C}_6\text{F}_5)_4]$ ^[20] reveal that $E_{1/2} = -2.09 \text{ V}$ vs. $\text{Fc}^{+/0}$. Assuming that $\epsilon_{\text{MTBE}} \cong \epsilon_{\text{Et}_2\text{O}} (4.24)$,^[19] $\Delta\Delta G^\circ(\text{MTBE-MeCN}) = -6.5 \text{ kcal/mol}$ and $\Delta E^\circ = 0.28 \text{ V}$ which also agrees with experiment ($\Delta E^\circ = 0.34 \text{ V}$). Therefore, **1** becomes more reducing as the dielectric constant decreases due to poorer solvent stabilization of the electrogenerated anion at the solution-electrode interface.

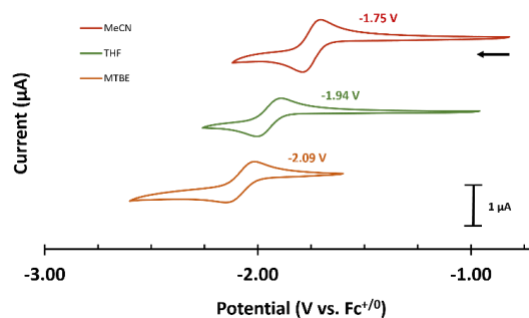
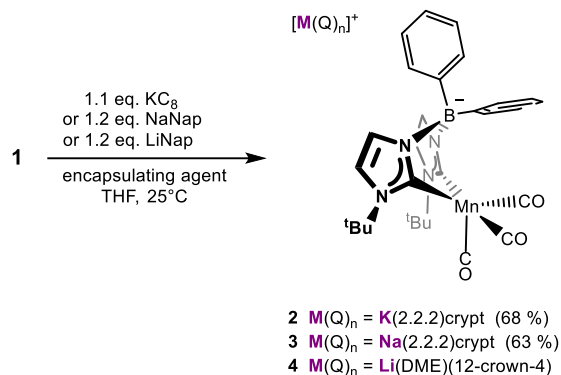


Figure 3. Cyclic voltammogram of **1** under three different conditions: MeCN, $0.1 \text{ M } [\text{nBu}_4\text{N}][\text{PF}_6]$ (red); THF, $0.1 \text{ M } [\text{nBu}_4\text{N}][\text{PF}_6]$ (green); MTBE, $0.075 \text{ M } [\text{nBu}_4\text{N}][\text{B}(\text{C}_6\text{F}_5)_4]$ (orange). In all cases, CVs were conducted under N_2 with 1 mM analyte at a scan rate of 0.1 V/s .

We sought to chemically reduce **1** by screening its reactivity with alkali metals. Red-orange **1** can be reacted with a slight excess of KC_8 , NaNap, or LiNap (Nap = Naphthalenide) in THF at 25°C to afford dark forest-green solutions. The addition of (2,2,2)cryptand or 12-crown-4 yielded the crystalline green salts $[\text{K}(2,2,2\text{-crypt})][\text{Ph}_2\text{B}(\text{t}^{\text{Bu}}\text{NHC})_2\text{Mn}(\text{CO})_3]$ (**2**), $[\text{Na}(2,2,2\text{-crypt})][\text{Ph}_2\text{B}(\text{t}^{\text{Bu}}\text{NHC})_2\text{Mn}(\text{CO})_3]$ (**3**), and $[\text{Li}(\text{DME})(12\text{-crown-4})][\text{Ph}_2\text{B}(\text{t}^{\text{Bu}}\text{NHC})_2\text{Mn}(\text{CO})_3]$ (**4**; Scheme 2).



Scheme 2. Syntheses of **2**, **3**, and **4**.

Complexes **2**, **3** and **4** have been characterized by single crystal X-ray diffraction and exhibit very similar structural features at the manganese center (Fig 4). The $\text{Mn}\text{---}\text{C}_{\text{ipso}}$ distance increases by approximately 0.860 Å (**2**), 0.765 Å (**3**), and 0.637 Å (**4**) when compared to **1** due to increased electronic repulsion between the metalloradical and ligand (Table 1). Furthermore, there is a weak interaction between the carbonyl oxygen (OB) and potassium (K2) atoms of **2** (2.963(4) Å; Fig 4) whereas for **3** and **4** there are no interactions between the encapsulated cation and CO ligands. A solid-state $\text{CO}\text{---}[\text{K}(2.2.2)\text{crypt}]^+$ interaction has been previously observed in a tricarbonylrhenium-bound quinoxaline salt ($\text{CO}\text{---}\text{K} = 2.900(5)$ Å) but in the analogous manganese salt no interaction was observed.^[21] A similar interaction was also observed when metallic rubidium was used as the reductant in the presence of (2.2.2)crypt to give an interatomic $\text{CO}\text{---}\text{Rb}$ distance of 3.126(2) Å between the terminal oxygen atom and rubidium cation.^[21]

Solid-state IR spectra of **2**, **3**, and **4** reveal nearly identical CO stretching frequencies that are all shifted 100–120 cm^{-1} lower than **1**, confirming the strong π backdonation effects upon reduction and that the counterion has little influence on the electronic structure at Mn (Table 1). UV-vis spectroscopy of **2** reveals a strong absorption maximum at 360 nm ($\epsilon_{360} = 1000 \pm 100 \text{ M}^{-1}\text{cm}^{-1}$), complementary to its perceived green colour (Fig S14).

Table 1. Selected bond distance comparisons and IR carbonyl stretches observed.

Complex	C≡O bond distance (Å)	Mn---C _{ipso} (Å)	C≡O stretches (cm ⁻¹)
1	1.150(3), 1.151(3), 1.161(3)	2.618(2)	2010,1928, 1881
2	1.166(5), 1.179(5), 1.174(6)	3.478(5)	1908,1808, 1765
3	1.168(5), 1.166(5), 1.174(5)	3.383(3)	1908,1801, 1771
4	1.165(6), 1.165(6), 1.165(6)	3.255(4)	1905,1801, 1764

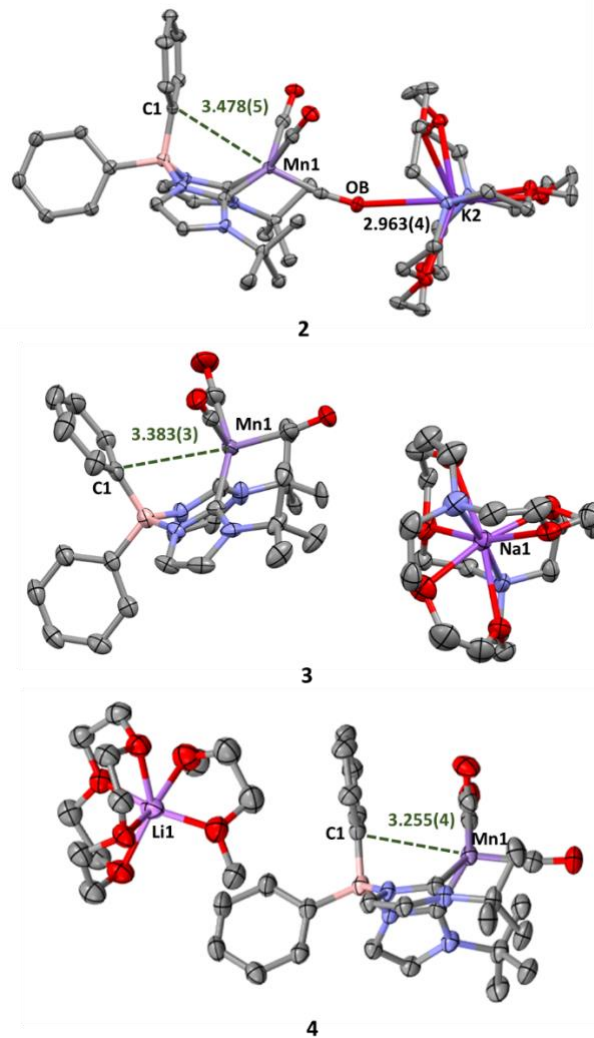


Figure 4. Molecular structures of **2**, **3**, and **4** with 50% probability ellipsoids; H atoms omitted for clarity. Cocrystallized solvent and additional molecules in the asymmetric unit of **4** are also omitted for clarity.

Solution-phase magnetic susceptibility of **2** ($2.06 \mu_B$, Evans' method)^[22] confirms the presence of one unpaired electron ($S = \frac{1}{2}$). The electron paramagnetic resonance (EPR) spectrum of **2** (Fig 5, left) demonstrates a rhombic symmetry with the simulation parameters $g = [2.018, 2.023, 1.998]$ and $A(^{55}\text{Mn}) = \pm [212, 149, 126]$ MHz. One g -factor component $g_z = 1.998$ is close to a free electron g -factor while two other components $g_{x,y}$ are slightly larger, as expected for $3d^7 \text{Mn}^0$ in a strong square-pyramidal ligand field with the unpaired spin residing on the $3d_{z^2}$ orbital.^[23,24] The EPR parameters of **2** are noticeably different from other reported square-pyramidal Mn^0 complexes, like $\text{Mn}(\text{CO})_5$ ($g_{\perp} = 2.038$, $g_{\parallel} = 2.000$; $A(^{55}\text{Mn}) = [A_{\perp} = -94, A_{\parallel} = 185]$ MHz)^[25] and $[\text{((n-Bu)}_3\text{P)}_2\text{-Mn}(\text{CO})_3]$ ($g_{\perp} = 2.036$, $g_{\parallel} = 2.007$; $A(^{55}\text{Mn}) = [A_{\perp} = -114, A_{\parallel} = 164]$ MHz),^[23] reflecting a different ligand field strength and coordination symmetry of the dicarbene ligand in **2** as compared to the CO and phosphine ligands in the above examples. Furthermore, a high hyperfine anisotropy, as observed in **2** and the above examples, is a signature feature of a Mn^0 redox state, distinguishing it from the Mn^{II} redox state with a low hyperfine anisotropy. The pronounced rhombicity of both g and $A(^{55}\text{Mn})$ in **2** indicates a low symmetry coordination geometry (C_{2v} or lower), promoting a sizeable admixture of $3d_{x^2-y^2}$ to the dominant $3d_{z^2}$ population.^[24] The DFT-calculated spin density for **2** (Fig 5, right) supports the predominately $3d_{z^2}$ metal-based radical character of the Mn^0 centre.

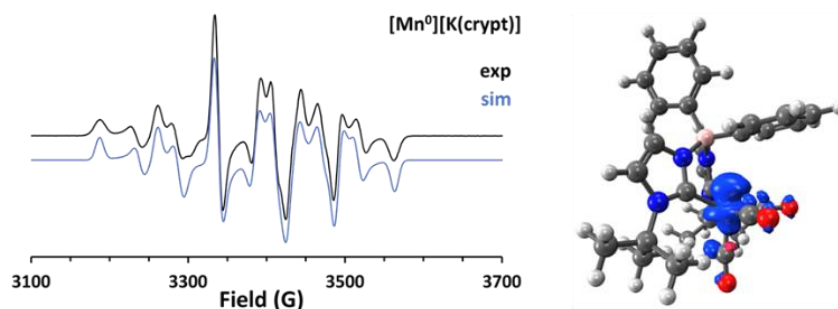


Figure 5. Left: X-band EPR spectrum of **2** (77 K, 2-MeTHF glass): experiment (black) and stimulation (blue). Right: Computed spin density plot of the Mn⁰ radical anion **2**⁻ at the TPSS-D3(BJ)/def-TZVP/CPCM(THF) level of theory, revealing predominantly 3d_{z²} spin localization (blue) consistent with the EPR data.

In summary, new anionic Mn⁰ complexes have been chemically synthesized from a redox-active Mn^I precursor using the chemical reductants KC₈, NaNap, or LiNap. All compounds have been structurally authenticated by single crystal X-ray diffraction and characterized by various spectroscopic methods to evaluate their structural and electronic properties. The arene ring of the borate-bridged bis(*N*-heterocyclic carbene) ligand plays an important role in stabilizing the Mn^I centre. The solvent-dependent redox behaviour can be rationalized using the Born equation, showing that media with a lower dielectric constant destabilize the manganate anion in solution. Upon 1e⁻ reduction, an increase in Mn⁰---C_{ipso} distance by 0.6–0.9 Å is observed and the low spin (*S* = ½) Mn⁰ complexes exhibit metal-based radical character, as confirmed by EPR spectroscopy and DFT calculations. The stoichiometric and electrocatalytic reactivity of this novel metalloradical complex with small molecules is ongoing.

This research was supported by a Rutgers-Newark startup grant and the Office of Advanced Research and Computing (OARC). The authors thank Dr. Pavel Kucheryavy (Rutgers-Newark) for NMR assistance.

References

1. R. Francke, B. Schille and M. Roemelt, *Chemical Reviews*, 2018, **118**, 4631-4701.
2. E. S. Wiedner, A. M. Appel, S. Raugei, W. J. Shaw and R. M. Bullock, *Chemical Reviews*, 2022, **122**, 12427-12474.
3. F. Franco, M. F. Pinto, B. Royo and J. Lloret-Fillol, *Angewandte Chemie International Edition*, 2018, **57**, 4603-4606.
4. M. Bourrez, F. Molton, S. Chardon-Noblat and A. Deronzier, *Angewandte Chemie International Edition*, 2011, **50**, 9903-9906.
5. J. M. Smieja, M. D. Sampson, K. A. Grice, E. E. Benson, J. D. Froehlich and C. P. Kubiak, *Inorganic Chemistry*, 2013, **52**, 2484-2491.
6. M. D. Sampson, A. D. Nguyen, K. A. Grice, C. E. Moore, A. L. Rheingold and C. P. Kubiak, *Journal of the American Chemical Society*, 2014, **136**, 5460-5471.
7. M. D. Sampson and C. P. Kubiak, *Inorganic Chemistry*, 2015, **54**, 6674-6676.
8. F. Hartl, T. Mahabiersing, P. Le Floch, F. Mathey, L. Ricard, P. Rosa and S. Zális, *Inorganic Chemistry*, 2003, **42**, 4442-4455.
9. D. W. Agnew, C. E. Moore, A. L. Rheingold and J. S. Figueroa, *Angewandte Chemie International Edition*, 2015, **54**, 12673-12677.
10. J. Cheng, Q. Chen, X. Leng, Z. Ouyang, Z. Wang, S. Ye and L. Deng, *Chem*, 2018, **4**, 2844-2860.
11. A. L. Narro, H. D. Arman and Z. J. Tonzetich, *Organometallics*, 2019, **38**, 1741-1749.
12. I. V. Shishkov, F. Rominger and P. Hofmann, *Organometallics*, 2009, **28**, 3532-3536.
13. A. P. Forshaw, R. P. Bontchev and J. M. Smith, *Inorganic Chemistry*, 2007, **46**, 3792-3794.
14. B. Cordero, V. Gómez, A. E. Platero-Prats, M. Revés, J. Echeverría, E. Cremades, F. Barragán and S. Alvarez, *Dalton Transactions*, 2008, 2832-2838.
15. S. S. Batsanov, *Inorganic Materials*, 2001, **37**, 871-885.
16. C. L. Perrin and T. J. Dwyer, *Chemical Reviews*, 1990, **90**, 935-967.
17. D. E. Richardson, *Inorganic Chemistry*, 1990, **29**, 3213-3217.
18. P. Atkins and J. D. Paula, *Atkins' Physical Chemistry*, W.H Freeman and Company, New York, 8th edn., 2006.
19. J. R. Rumble, "Physical Constants of Organic Compounds" in *CRC Handbook of Chemistry and Physics 103rd Edition*, CRC Press/Taylor & Francis Boca Raton, FL, 2022.

20. R. J. LeSuer and W. E. Geiger, *Angewandte Chemie International Edition*, 2000, **39**, 248-250.
21. S. Choua, J.-P. Djukic, J. Dalléry, A. Bieber, R. Welter, J.-P. Gisselbrecht, P. Turek and L. Ricard, *Inorganic Chemistry*, 2009, **48**, 149-163.
22. D. F. Evans, *Journal of the Chemical Society (Resumed)*, 1959, 2003-2005.
23. G. B. Rattinger, R. L. Belford, H. Walker and T. L. Brown, *Inorganic Chemistry*, 1989, **28**, 1059-1066.
24. B. R. McGarvey, *Canadian Journal of Chemistry*, 1975, **53**, 2498-2511.
25. J. A. Howard, J. R. Morton and K. F. Preston, *Chemical Physics Letters*, 1981, **83**, 226-228.

Table of Contents Graphic

